AIP | Physics of Plasmas

Two-dimensional hybrid Monte Carlo–fluid modelling of dc glow discharges: Comparison with fluid models, reliability, and accuracy

E. Eylenceoğlu, I. Rafatov, and A. A. Kudryavtsev

Citation: Physics of Plasmas (1994-present) **22**, 013509 (2015); doi: 10.1063/1.4906361
View online: http://dx.doi.org/10.1063/1.4906361
View Table of Contents: http://scitation.aip.org/content/aip/journal/pop/22/1?ver=pdfcov
Published by the AIP Publishing

Two-dimensional hybrid Monte Carlo–fluid modelling of dc glow discharges: Comparison with fluid models, reliability, and accuracy

E. Eylenceoğlu,[1] I. Rafatov,[1,a)] and A. A. Kudryavtsev[2]
[1]*Department of Physics, Middle East Technical University, Ankara, Turkey*
[2]*Saint Petersburg State University, St.Petersburg, Russia*

(Received 2 November 2014; accepted 7 January 2015; published online 22 January 2015)

Two-dimensional hybrid Monte Carlo–fluid numerical code is developed and applied to model the dc glow discharge. The model is based on the separation of electrons into two parts: the low energetic (slow) and high energetic (fast) electron groups. Ions and slow electrons are described within the fluid model using the drift-diffusion approximation for particle fluxes. Fast electrons, represented by suitable number of super particles emitted from the cathode, are responsible for ionization processes in the discharge volume, which are simulated by the Monte Carlo collision method. Electrostatic field is obtained from the solution of Poisson equation. The test calculations were carried out for an argon plasma. Main properties of the glow discharge are considered. Current-voltage curves, electric field reversal phenomenon, and the vortex current formation are developed and discussed. The results are compared to those obtained from the simple and extended fluid models. Contrary to reports in the literature, the analysis does not reveal significant advantages of existing hybrid methods over the extended fluid model. © *2015 AIP Publishing LLC*.
[http://dx.doi.org/10.1063/1.4906361]

I. INTRODUCTION

Glow discharges find applications as plasma sources in many industrial processes, among which are surface modification, etching and deposition, lighting and lasers, etc.[1] The design and optimization of the discharge parameters in these applications require a good insight into the physical processes involved in glow discharges. Numerical modelling has proved to be a powerful technique for this purpose.

Glow discharge is a very complicated medium for numerical modelling. One of the reasons for this is the significantly distinct time, space, and energetic scales of different processes in the plasma. Even the seemingly simple case of a dc glow discharge, sustained between two parallel planar electrodes, turns out to be a rather complex problem. A self organization of this discharge, whose "anatomy" includes specific regions such as a cathode layer, negative glow, Faraday space, positive column, etc., is also worthy of special attention. It should be mentioned in this connection that some phenomena occurring in the plasma of the glow discharge, such as field reversal[2] and vortex current formation,[3] are still not understood sufficiently well. All of these impose heavy demands on a numerical model in that it must be adequate to take discharge plasma properties properly into account.

Numerical modelling techniques for glow discharges are still under intensive investigation.[4–16] In general terms, these approaches can be classified into fluid, hybrid, and kinetic (particle) methods. Fluid models of glow discharges usually contain continuity equations for charged species (electrons and ions) with drift-diffusion approximation for fluxes, which are equipped with the Poisson equation for the electric field. Simple fluid models employ a local field approximation (LFA), for which transport (mobility and diffusion) coefficients as well as the ionization rates are determined as functions of the reduced electric field. These models seem to be capable in describing basic properties of the discharge in a self-consistent way. However, it turns out that models based on LFA *a priori* can lead to a physically incorrect picture. The reason is that simple fluid models are unable to take account of ionization properly in the negative glow of the discharge, the region where electric field is weak and where the ionization is non-local.[2,11,17]

To overcome the drawbacks associated with LFA and to partially take account of nonlocal effects in the plasma, extended fluid model was suggested in Ref. 11 and its various modifications were applied in Refs. 7, 11, and 18. Within this model, the transport and kinetic coefficients of the electrons are determined as functions of the electron temperature rather than local value of the electric field, by using tabulated data obtained from solution of the kinetic Boltzmann equation. Spatial profile of the electron temperature is found from the electron energy equation, which incorporates not only volume processes but also transfer by heat conduction. In these situations, the electron heating source in the plasma is nonlocal: heating is due to the heat flux from the cathode layer, where main Joule heating occurs.

Within the kinetic particle methods, which provide quantitatively accurate results, particle species composing the plasma are simulated by super particles.[4,6,19] However, this approach requires cumbersome computational efforts, because a reasonably large number of super particles must be involved in simulations to obtain accurate and noise free results.

To improve accuracy of fluid models and reduce computational difficulties associated with the kinetic and particle

a)Electronic mail: rafatov@metu.edu.tr.

methods, a hybrid Monte Carlo–fluid model, which is partially fluid and partially kinetic, is an option.[7,20–22] Within this model, electrons are separated into two groups, namely, fast and slow electrons. While fast electrons are simulated as particles with Monte Carlo method to account for collisions, slow electrons are described by the fluid model.

In fact, both numerical approaches proved to be workable to model glow discharges, namely, extended fluid model and hybrid model.

Comparison of different one-dimensional (1D) fluid and hybrid models, as applied to low-pressure dc glow discharges, was done in Ref. 9. Their results indicated an inadequacy of simple fluid models in description of the cathode region of glow discharges. The best agreement with experimental data has been found using the hybrid model. However, in our view, advantages of hybrid model are constrained by introducing the characteristic energy of slow (bulk) electrons T_e as an input parameter, which in reality acts as a fitting parameter. By this, it is meant that this model is not self-consistent, which to a great extent degrades its worth. An extended fluid model, in turn, provides self-consistent description of the properties and structure of the discharge. However, within this model, nonlocality of plasma is taken approximately into account, which leads to an overestimation of the electron temperature.[5] Therefore, comparison of the two most commonly used (the extended fluid and the hybrid) models shows that both of these have their advantages and shortcomings.

In this work, we develop and apply a two-dimensional (2D) hybrid Monte Carlo–fluid numerical code to model dc glow discharge. The details of the model and numerical method, applied to the Monte Carlo and fluid parts, are described in Sec. II. Numerical results and discussions are presented in Sec. III. First, in order to validate the numerical code, we carried out calculations under conditions of Ref. 9 within 1D approximation. Next, we computed the current-voltage curves of the discharge. Results from simple and extended fluid models are also included. Furthermore, we discuss the field reversal phenomena and consider properties of the discharge and vortex currents formation as obtained within 2D simulations. Finally, in Sec. IV, a brief summary of the study is given.

II. THE HYBRID MONTE CARLO–FLUID MODEL

The hybrid Monte Carlo–fluid model for a glow discharge is based on the partition of the electron population into two groups, namely, the low energetic (slow) and high energetic (fast) groups.[23] Ions and slow electrons are described within the fluid model using the drift-diffusion approximation for particle fluxes. Electric field is obtained from the solution of the Poisson equation. Fast electrons, which are simulated by a suitable number of super particles (usually several hundreds) emitted from cathode into the discharge volume, are responsible for the ionization processes in the plasma. Effects of collisions are simulated by the Monte Carlo Collision (MCC) method that allows to take the nonlocal transport of electrons in the cathode region properly into account.[21,23] Electron elastic, excitation, and ionization collisions with the background neutral gas particles are included in the model, while the electron–electron and electron–ion collisions are ignored.

A. Fluid part of the model

Fluid part of the model consists of continuity equations for slow electrons and ions[4]

$$\frac{\partial n_{se}}{\partial t} + \nabla \cdot \mathbf{\Gamma}_{se} = S_{se}, \tag{1}$$

$$\frac{\partial n_i}{\partial t} + \nabla \cdot \mathbf{\Gamma}_i = S_i, \tag{2}$$

coupled with the Poisson equation for the electric field

$$\nabla^2 \varphi = -\frac{e}{\varepsilon_0}(n_i - n_e). \tag{3}$$

Here n denotes the particle density, $\mathbf{\Gamma}$ the particle flux density, φ the electric potential. The total electron density is $n_e = n_{se} + n_{fe}$. The source terms S_{se} and $S_i = S_{se} + S_{fe}$ in the continuity equations (1) and (2) describe the generation rates of slow electrons and ions, which are obtained from the MCC simulation of fast electrons. Subscripts *se* and *fe* refer to slow and fast electrons, and *i* to ions. Flux densities are expressed in the drift-diffusion form

$$\mathbf{\Gamma} = -D\nabla n \pm \mu \mathbf{E}\, n, \tag{4}$$

where D and μ denote the diffusion and mobility coefficients, $\mathbf{E} = -\nabla\varphi$ is the electric field vector.

B. MCC simulation of fast electrons

The MCC cycle of the hybrid code uses as an input parameter the electric field profile obtained from the fluid part of the code in the previous time step and generates spatial distributions of the ionization functions for positive ions and slow electrons, which are then employed as source terms for the respective continuity equations in the next time step.

Within the MCC cycle, the fast electrons are tracked in the discharge volume as they move in response to the electric field and make random collisions (elastic and inelastic) with the background neutral gas atoms. The positions $\mathbf{r}_k$ and velocities $\mathbf{v}_k$ of these particles between the collisions are updated using equations

$$\mathbf{v}_k^{m+1} = \mathbf{v}_k^m + \mathbf{a}_{\mathrm{eff},k}^m \Delta t, \tag{5}$$

$$\mathbf{r}_k^{m+1} = \mathbf{r}_k^m + \mathbf{v}_k^m \Delta t + 0.5\, \mathbf{a}_{\mathrm{eff},k}^m \Delta t^2, \tag{6}$$

where components of the effective acceleration $\mathbf{a}_{\mathrm{eff}}$ are determined in the form[21]

$$a_{\mathrm{eff},x} = -\frac{e}{m_e}\left(E_x + 0.5\, v_x \frac{\partial E_x}{\partial x}\Delta t\right), \tag{7}$$

$$a_{\mathrm{eff},y} = -\frac{e}{m_e}\left(E_y + 0.5\, v_y \frac{\partial E_y}{\partial y}\Delta t\right). \tag{8}$$

Here, m indicates the time level and k the electron index. Δt is the time step size, e the electron charge, m_e the electron mass, v_x and v_y are x and y components of the velocity vector.

For a small time step Δt, collision probability P_c of an electron is expressed in the form

$$P_c = 1 - e^{-N_g \sigma_{tot}(v_r) v_r \Delta t}, \tag{9}$$

where N_g is density of the background neutral gas, $\sigma_{tot} = \sigma_{el} + \sigma_{ex} + \sigma_{iz}$ is velocity (or energy) dependent total collision cross section taking into account the elastic, excitation, and ionization collisions of electrons with the background neutral gas atoms, and v_r is relative velocity. The cross-section set is presented in Fig. 1. For collisions between fast electrons and neutral gas particles, relative velocities v_r are equal to the electron velocities.[4] For a group of electrons, the probability of collisions can be obtained by averaging over the velocity distribution, expressed in the form

$$P_c = 1 - e^{-N_g <\sigma_{tot}(v) v> dt}. \tag{10}$$

When this number is multiplied with the total number of electrons involved in the MCC cycle, the result gives the number of electrons colliding with background gas atoms.[4,22] The criterion of making a collision as well as making a specific type of collision (elastic, ionization, or excitation) is determined by using random numbers uniformly distributed between 0 and 1.

Fast electrons lose their energy in inelastic (ionization and excitation) collisions with neutral particles as they proceed along their trajectories in the volume. We classified an electron having nonzero probability to make such a collision as a fast electron. This is the case if the total (kinetic + potential) energy of the electron is greater than the threshold energy of excitation, $E_{kin} + e(\varphi_{max} - \varphi) \geq E_{ex}$. An electron passes from the fast to the slow electron group if its total energy happens to be lower than E_{ex}.

After all fast electrons within MCC cycle have escaped from the volume or converted to slow electrons, positions of relative events (ionizations, transitions to slow electron group) are processed and numbers of ions and slow electrons, N_i and N_{se}, created within every grid cell ΔV are obtained. (ΔV is Δx in 1D and $\Delta x \Delta y$ in 2D case, Δx and Δy are grid cell sizes in x and y directions.) A profile per one primary electron is obtained by normalizing with N_0, the total number of primary electrons emitted from cathode surface in the MCC cycle. Actual source profiles are developed by multiplying with the actual number of electrons, emitted from cathode within the previous fluid cycle, so that the source functions for ions and slow electrons obtain the form

$$S_{i,se} = j_e \frac{1}{N_0} \frac{N_{i,se}}{\Delta V}, \tag{11}$$

where j_e is the electron current density on the cathode. In 1D, using condition of secondary electron emission (will be introduced below), $j_e = j/(1 + 1/\gamma)e$, where j is the total current density, γ the emission coefficient, and e the electron charge.[7,9] For 2D case, j_e becomes a function of transversal coordinate y and is determined again from the conditions for secondary electron emission, using current density distribution on the cathode, calculated in the fluid cycle in the previous time step.

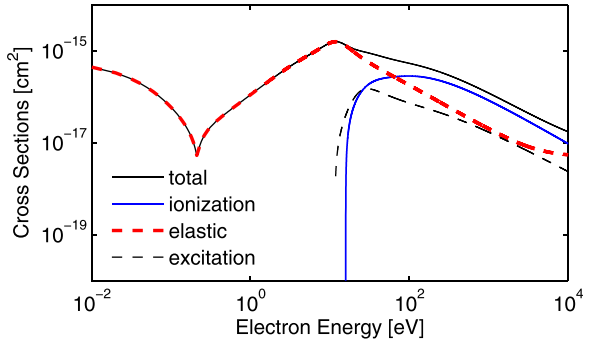

FIG. 1. Elastic, excitation, ionization, and total cross-sections for electrons in argon gas.[24]

C. Numerical procedure for the fluid part of the model

Continuity equations introduced in Sec. II A are discretized using the control volume method, so that the corresponding finite-difference equations in 2D rectangular domain (x, y) obtain the form

$$\frac{n_{i,j}^{k+1} - n_{i,j}^{k}}{\Delta t} \Delta x \Delta y + \left(\Gamma_{x\,i,j+1/2}^{k+1} - \Gamma_{x\,i,j-1/2}^{k+1} \right) \Delta y + \left(\Gamma_{y\,i+1/2,j}^{k+1} - \Gamma_{y\,i-1/2,j}^{k+1} \right) \Delta x = S_{i,j}^{k} \Delta x \Delta y. \tag{12}$$

Indices i and j parameterise grid points positions in y and x directions, k is a time level. The flux densities Γ are approximated with the exponential scheme (also known as Scharfetter-Gummel method)[25]

$$\Gamma_{x\,i,j+1/2}^{k+1} = \mu_{i,j+1/2} E_{x\,i,j+1/2} \frac{n_{i,j}^{k+1} - n_{i,j+1}^{k+1} e^{-P_{i,j+1/2}}}{1 - e^{-P_{i,j+1/2}}}, \tag{13}$$

$$\Gamma_{y\,i+1/2,j}^{k+1} = \mu_{i+1/2,j} E_{y\,i+1/2,j} \frac{n_{i,j}^{k+1} - n_{i+1,j}^{k+1} e^{-P_{i+1/2,j}}}{1 - e^{-P_{i+1/2,j}}}. \tag{14}$$

Here, P denotes the Peclet number

$$P_{i,j+1/2} = \frac{\mu_{i,j+1/2} E_{x\,i,j+1/2}}{D_{i,j+1/2}} \Delta x, \tag{15}$$

$$P_{i+1/2,j} = \frac{\mu_{i+1/2,j} E_{y\,i+1/2,j}}{D_{i+1/2,j}} \Delta y. \tag{16}$$

Equations (12) for slow electrons and ions are solved by the Tridiagonal Matrix Algorithm (TDMA) line by line in the longitudinal x–direction (Method of Lines[25]). When written in the way suitable for solution by TDMA, these equations obtain the form

$$a_{i,j}^{k} n_{i,j}^{k+1} = b_{i,j}^{k} n_{i,j-1}^{k+1} + c_{i,j}^{k} n_{i,j+1}^{k+1} + \tilde{S}_{i,j}^{k}, \tag{17}$$

where $\tilde{S}_{i,j}^{k}$ in the right-hand side contains terms from neighbouring grid points from the transverse y–direction

$$\tilde{S}_{i,j}^k = d_{i,j}^k n_{i-1,j}^k + e_{i,j}^k n_{i+1,j}^k + S_{i,j}^k. \quad (18)$$

For the Poisson equation, the discretized equations are written in the form

$$A_j^k \Phi_j^k = B_j^k \Phi_{j-1}^k + C_j^k \Phi_{j+1}^k + \Omega_j^k, \quad (19)$$

and solved by the Block-Tridiagonal Matrix Algorithm (see Ref. 26, p. 56). Here A, B, and C are $N_y \times N_y$ matrices, Φ and Ω are $N_y \times 1$ column matrices.

The stationary solution of the problem is obtained by successive iterations of the fluid and Monte Carlo cycles of the model. Time discretization is partly implicit and partly explicit because the electric field profile and hence the transport coefficients (which are functions of the electric field) are taken from the previous time step. This imposes restrictions on the time step Δt: it is limited by the time scales caused by the (i) Courant-Friedrichs-Lewy condition, (ii) by the period of the electron plasma oscillations, and (iii) by the dielectric relaxation time

$$\tau_{DR} = \frac{\varepsilon_0}{e\mu_e n_e + e\mu_i n_i}. \quad (20)$$

The last condition imposes the strongest restriction on the time step, especially when the plasma density is relatively high. For example, for a density about $n = 10^{10}\,\mathrm{cm}^{-3}$, τ_{DR} is on the order 10^{-10} s.

D. Boundary conditions

Calculations are carried out in the rectangular (x, y) region with a uniform grid in each direction. Cathode and anode are located at $x = 0$ and $x = L_x$, respectively.

Boundary condition for the electric potential is the grounded potential on the cathode and voltage V_a applied on the anode. On the dielectric side walls, which are assumed to be perfect absorbers, electric field is determined from the Gauss law, $\hat{\mathbf{n}} \cdot \mathbf{E} = -\sigma/\varepsilon_0$, where surface charge density σ is determined from the equation

$$\frac{\partial \sigma}{\partial t} = e(\mathbf{\Gamma}_i - \mathbf{\Gamma}_e) \cdot \hat{\mathbf{n}}, \quad (21)$$

where $\hat{\mathbf{n}}$ is normal unit vector outward to the wall surface.

Boundary conditions for slow electrons and ions on the electrodes and side walls are defined by the directed fluxes[8]

$$\hat{\mathbf{n}} \cdot \mathbf{\Gamma}_e = \frac{1}{4} n_e v_e - \alpha_e \mu_e n_e (\hat{\mathbf{n}} \cdot \mathbf{E}) - \beta_e \gamma |\hat{\mathbf{n}} \cdot \mathbf{\Gamma}_i|, \quad (22)$$

$$\hat{\mathbf{n}} \cdot \mathbf{\Gamma}_i = \frac{1}{4} n_i v_i + \alpha_i \mu_i n_i (\hat{\mathbf{n}} \cdot \mathbf{E}), \quad (23)$$

where $v_{i,e} = \sqrt{8\pi T_{i,e}/e m_{i,e}}$ are the electron and ion thermal speeds. The last term in Eq. (22) contributes to the secondary electron emission from the walls, bombarded by energetic ions, with emission coefficient γ. Parameter $\beta_e = 1$ on the cathode and 0 otherwise. Parameters $\alpha_{i,e}$ regulate drift fluxes to the walls: $\alpha_{i,e} = 1$ if the flux is directed onto the wall and 0 otherwise.

III. RESULTS AND DISCUSSIONS

Simulations are carried out for discharge in argon gas at pressure $p = 1$ Torr and a constant temperature $T_g = 0.025$ eV. Dimensions of the discharge cell in longitudinal x and transverse y directions are $L_x = L_y = 1$ cm. Constant mobility and diffusion coefficients are used for slow electrons, $\mu_e = 3 \times 10^5\,\mathrm{cm}^2\mathrm{s}^{-1}\mathrm{V}^{-1}$ and $D_e = \mu_e T_e$, where $T_e = 0.3$, 1 and 3 eV.[9] Ion temperature is assumed to be equal to the temperature of the background gas, $T_i = T_g$. Mobility and diffusion coefficients of ions are determined as functions of reduced electric field as in Refs. 27 and 28.

We first verify hybrid Monte Carlo–fluid code by carrying out 1D calculations and comparing the results with those from Ref. 9. We also present results for simple fluid and extended fluid models obtained under the same conditions. Next, we present 2D modelling results, compare current-voltage curves, obtained within 1D and 2D models and from the experiments, discuss a field reversal phenomena and formation of vortex currents in the plasma.

A. Validation of 1D hybrid Monte Carlo–fluid code

In order to verify the numerical code, we performed 1D simulations under conditions of Ref. 9, for argon at $p = 1$ Torr, a gap between the electrodes of $L = 1$ cm, an applied voltage $V_a = 250$ V, $T_e = 1$ eV, and secondary emission coefficient $\gamma = 0.06$. In order to fit the results obtained in Ref. 9, we applied boundary conditions not as described in Sec. II D but in a more crude way: $n_i = n_e = 0$ on the anode, $\partial n_i/\partial z = 0$ and a secondary emission condition (22) on the cathode. Results of the calculation (profiles of the electron and ion density, electric field, and ionization source) are presented in Fig. 2. As can be seen, profiles of the particle densities (panel (a)) and the electric field (panel (b)) fit perfectly with the results obtained in Ref. 9. A discrepancy in the ionization function (panel (c)), which appears in the direction closer to the anode, may be caused by a different number of super electrons involved in the Monte-Carlo cycle and also by different criteria used for separation of electrons into fast and slow groups. However, this has no effect on the plasma properties, as evident from the panels (a) and (b).

In order to demonstrate the effect of different modelling approaches on the discharge properties, we added in Fig. 2 results obtained under the same parameter regime ($V_a = 250$ V) but using the simple fluid and extended fluid models. (In the simple fluid model, ionization source is approximated by the Townsend formula. In the case of the extended fluid model, the model and plasma-chemical reactions are defined exactly as in Ref. 5.) The current densities corresponding to models in Fig. 2 are, respectively, 0.8 and 1.74 mA/cm^2 in the case of the hybrid and extended fluid models and 0.11 mA/cm^2 in the case of the simple fluid model. The last one appears to be about one-tenth that for the hybrid and extended fluid models so that the corresponding discharge regime falls into a different region of CVC (current-voltage characteristics) curve.

Wide scatter in the properties of different fluid methods as well as in the properties of fluid and hybrid models (reported in Ref. 9) seem to be caused by comparison of

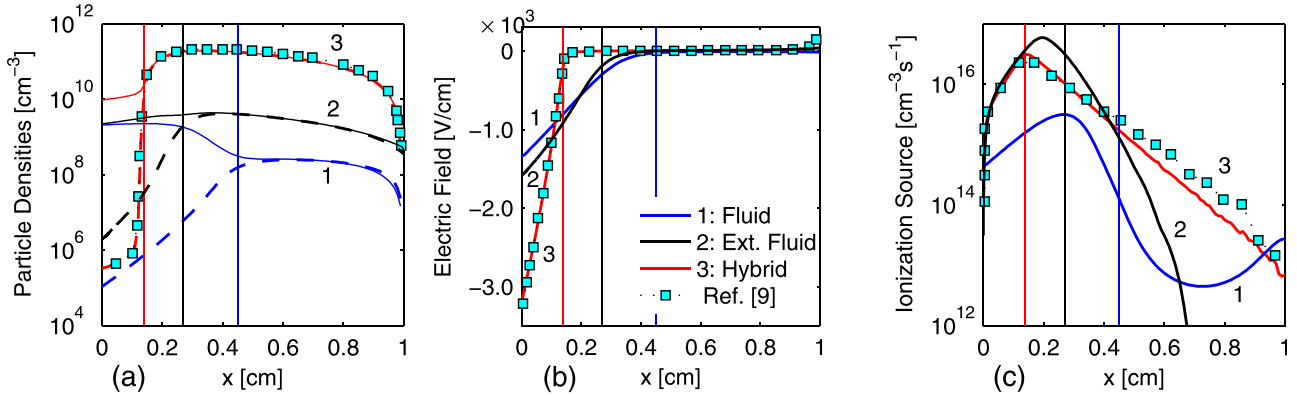

FIG. 2. Validation of the 1D hybrid code. (a) Electron and ion densities, (b) electric field, and (c) ionization source profiles. Squares correspond to computed results from Ref. 9. Vertical lines indicate cathode sheath thicknesses. $p = 1$ Torr, $T_e = 1$ eV, $\gamma = 0.06$, $L = 1$ cm, $V_a = 250$ V.

discharges at essentially different regimes; discharge properties should be computed not at the same applied voltage but the discharge current. For a more proper comparison, Fig. 3 illustrates the same properties as in Fig. 2, which were obtained in the case of the same discharge current density, $0.8\,\mathrm{mA/cm^2}$, rather than voltage. (Here we applied boundary conditions as described in Sec. II D.) Voltages needed to sustain a discharge with this current density vary from 255 V (in the case of the hybrid model) to 223 V and 706 V for the extended and simple fluid models, respectively. Vertical lines in Figs. 2 indicate the borders between the cathode sheath and negative glow regions of the discharge, for different models. Points separating these regions were determined from the condition $n_e = 0.5 n_i$.

Compared to results in Fig. 2, the discharge properties in Fig. 3 computed by fluid models lead to qualitatively similar results, with much closer plasma densities, almost equal cathode layer thicknesses and ionization profiles which are similar in the cathode layer and differ in the negative glow. However, these results diverge significantly from those obtained from the hybrid model for the plasma density and the thickness of the cathode layer.

Electron transport in the plasma of the glow discharge cannot be determined as a function of local value of the electric field.[2,17] This feature is referred to as nonlocality of ionization in the plasma. In glow discharge models, which describe this feature adequately, the ionization events are taken into account properly within in the negative glow of the plasma, despite a weak electric field in that region.[2,10] As can be seen from Fig. 3(c), the hybrid model and partially extended fluid model are able to predict the ionization function adequately, while the simple fluid model does not. The hybrid model takes into account the nonlocal character of the electron transport by means of the particle MCC simulation of the fast electron kinetics. Within the extended fluid model, nonlocality of electrons transport is partially incorporated through the electron energy balance, by the convective heat flux from the cathode layer, where main Joule heating occurs.[11,18]

Notice that in addition to the case with $T_e = 1$ eV shown in Fig. 2, Fig. 3 also contains results computed by the hybrid model for $T_e = 0.3$ and 3 eV. The effect of T_e on the particle number density is as expected: the temperature T_e varies inversely to the slow electron density n_e (see Fig. 3(a)). In order to sustain a discharge with current density $J = 0.8\,\mathrm{mA/cm^2}$, the applied voltage V_a varies as 259, 255, and 243 V for $T_e = 0.3$, 1, and 3 eV, respectively. The effect of T_e on the electric field and ionization source is not noticeable (see Figs. 3(b) and 3(c)). The reason is that under the same current density, the charge density profiles for $T_e = 0.3$, 1, and 3 eV appear very close to each other in the cathode region of the discharge, so that the resulting electric field profiles become almost identical (Fig. 3(b)). The Monte Carlo simulation of fast electrons, which is

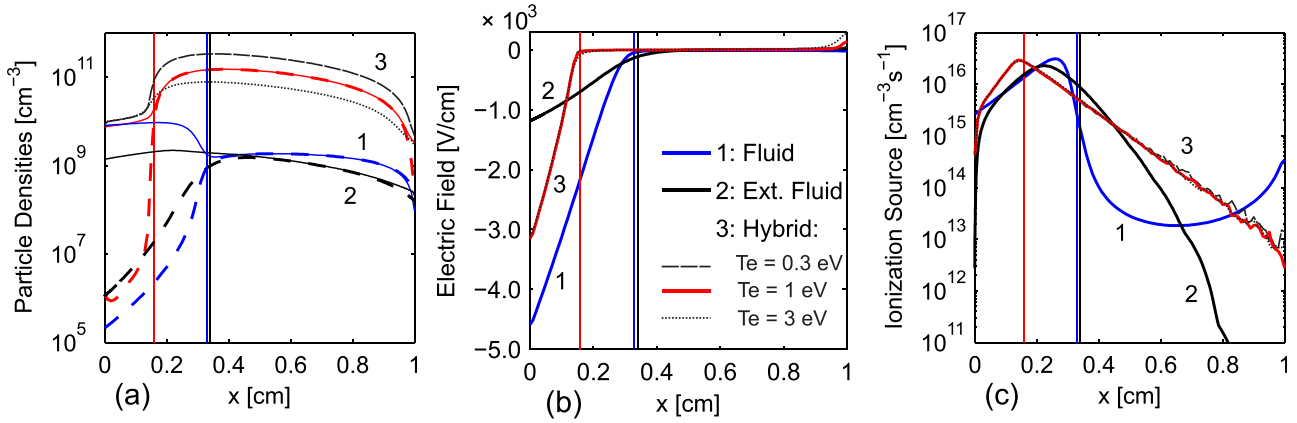

FIG. 3. The same plasma properties as in Fig. 2 computed at the same current density. (a) Electron and ion densities, (b) electric field, (c) ionization source. Vertical lines indicate cathode sheath thicknesses. $p = 1$ Torr, $T_e = 0.3$, 1, and 3 eV, $\gamma = 0.06$, $L = 1$ cm, $J = 0.8\,\mathrm{mA/cm^2}$.

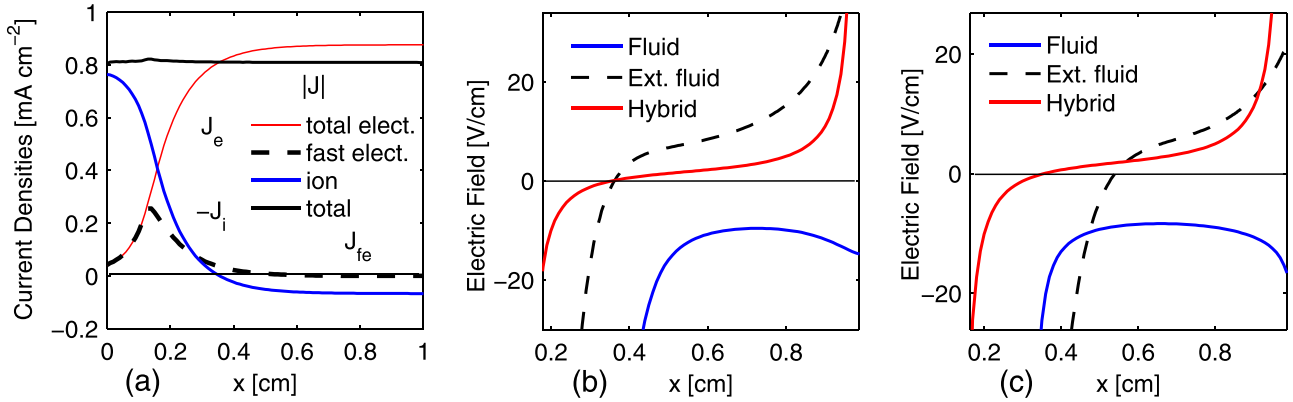

FIG. 4. 1D hybrid model. (a) Ion current density J_i, total electron current density J_e, fast electron current density J_{fe}, and total current density J (conditions are the same as in Fig. 2), (b) closer look to the field reversal in Fig. 2(b), (c) closer look to the field reversal in Fig. 3(b).

independent from T_e, employs the electric field profile as an input parameter. Correspondingly, the ionization functions, which shapes are determined from the Monte Carlo simulations, become coinciding very closely. As a particular result, it is impossible for the hybrid model to reproduce the results of the extended fluid model by a suitable choice of the slow electron temperature T_e.

B. Electric field reversal

An interesting effect of nonlocal ionization in the plasma of glow discharges, which adequate models reveal, is that the electric field is reversed at a certain point of the negative glow. As illustrated in Figs. 4(b) and 4(c), hybrid and extended fluid models exhibit a field reversal, which is not the case for the simple fluid model. Notice that the ion current reverses direction to the anode ($-J_i < 0$) exactly at the electric field reversal point (Figs. 4(a) and 4(b)). The uniform profile of the total current density J in Fig. 4(a) indicates a correct implementation of the numerical model.

The computed field reversal point is in excellent agreement with that estimated according to Ref. 17. In Ref. 17, the nonlocal ionization source was approximated by the function

$$S_i(x) = \begin{cases} \alpha_c \Gamma_{e0} \exp(\alpha_c x) & \text{if } x < d_c, \\ \max(S_i) \exp(-(x-d_c)/\lambda) & \text{if } x \geq d_c, \end{cases} \quad (24)$$

where $\alpha_c = \alpha_c(U_a/d_c)$ is the Townsend coefficient defined as function of the mean electric field over the cathode layer, U_a and d_c are the potential drop and thickness of the cathode layer, λ is the rate of the ionization source decay (which appears to be about the decay rate of the fast electron flux in the negative glow), and $\max(S_i)$ is the maximum value of the ionization source (it occurs about the cathode sheath boundary). We used computed ionization source profile (obtained by 1D hybrid model, Fig. 2(c)) to fit parameters in Eq. (24): $\alpha_c = 1800\,\text{cm}^{-1}$, $d_c = 0.15\,\text{cm}$, and $\lambda = 0.10\,\text{cm}$. Using the equation from Ref. 17

$$x_m = d_c - \lambda \ln\left\{\frac{\lambda}{L-d_c}\left[1 - \exp\left(-\frac{L-d_c}{\lambda}\right)\right]\right\}, \quad (25)$$

where the field reversal point x_m is defined in terms of d_c, λ, and the discharge gap L, we obtain $x_m = 0.364\,\text{cm}$. This is in perfect agreement with the position of the field reversal predicted by the hybrid model, which is 0.360 cm.

C. Current-voltage curves

The current-voltage curves (CVC) are the important integral characteristics of the glow discharges. Computed CVC's obtained from 1D and 2D hybrid codes with secondary electron emission coefficient $\gamma = 0.06$ are presented in Fig. 5(a). Voltages in the case of 2D computations are slightly higher than those obtained in 1D due to charged particles escaped from the side walls.[29] This figure includes also CVC computed from 1D hybrid model from Ref. 7, which is in close agreement with our 1D result.

In the glow discharge models, secondary emission coefficient γ is one of the main sources of uncertainty. It is also used in the discharge models as a fitting parameter to make the computed data fit the measured ones.[7] In order to demonstrate the effect of this coefficient on the modelling results, Fig. 5(a) contains also CVC computed from the hybrid model with emission coefficient dependent on the reduced electric field, $\gamma = 0.01(E/N)^{0.6}$ suggested in Ref. 30. In this case, CVC has a slope essentially different from those obtained with constant $\gamma = 0.06$. This, however, appears to be much closer to the measured CVC's from Refs. 31 and 32 as shown in Fig. 5(b).

Notice that Fig. 5 also includes CVC's obtained from fluid models. These figures demonstrate apparent failure of the simple fluid models to predict integral characteristics of the discharge. As can be seen, CVC curves computed from the simple fluid model are significantly further apart from those obtained from the measurements as well as from the hybrid and extended fluid models. Compared to CVC curves computed from the extended fluid model, CVC's from the hybrid model appear to be relatively closer to those from the measurements. However, the analysis does not reveal significant advantages of the hybrid method over the extended fluid model as reported in Ref. 9. Accuracy of the integral characteristics for both hybrid and extended fluid models is a matter of fitting parameter γ as demonstrated in Fig. 5. Concerning the local characteristics, hybrid models are obviously capable to describe cathode region more accurately.[9] However, hybrid

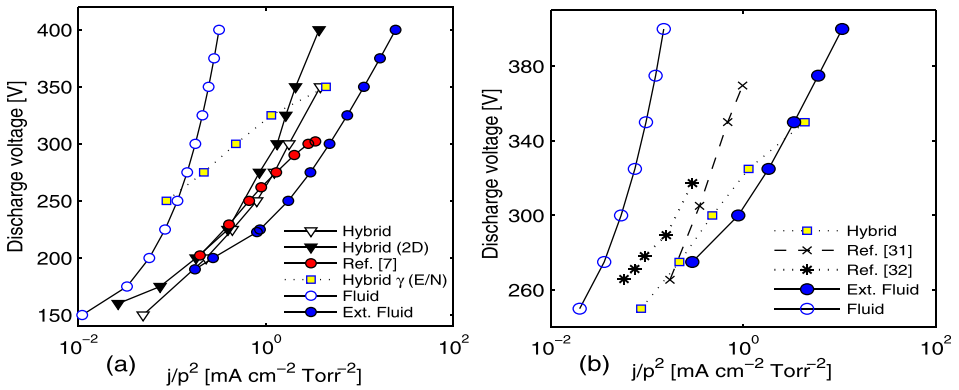

FIG. 5. (a) CVC curves obtained from hybrid (1D and 2D) and fluid (1D) models, emission coefficients $\gamma = 0.06$, (b) comparison of CVC's computed from 1D hybrid and fluid models with $\gamma = 0.01(E/N)^{0.6}$ and measured CVC's from Refs. 31 and 32. Notice that CVC with electric field dependent γ obtained from 1D hybrid model (yellow squares) appears in both panels (a) and (b).

model suffers from the disadvantage to set an additional input (fitting) parameter, namely, the electron temperature T_e (which is inversely related to computed plasma density), which also contributes to uncertainty of the model.

D. Current flows and vortex formation

Effects of 2D geometry on the discharge properties obtained from the hybrid model are demonstrated in Figs. 6–8. Figure 6(a) contains profiles of longitudinal x components of the current densities, averaged in transversal y direction. Flat profile of the total current density in Fig. 6(a) (as well as in the case of 1D model, in Fig. 4(a)) implies the charge conservation and hence exhibits correct implementation of the method.

Figure 6(b) contains profiles of the cathode sheath thickness d_c, field reversal point d_m, and local maxima of the ionization source, the ion density and fast electron density as functions of transverse coordinate y. (Profile for maximum of the slow electron density coincides very closely with profile of the ion density and is not shown in the figure.) The non-homogeneity of these profiles over the discharge cross-section is noteworthy. The reason has to do with the effects of side walls, and hence it indicates the limitations of 1D models for glow discharges. Therefore, adequate description of the discharge must be at least two-dimensional and take properly account of losses of charged and excited particles in the transverse direction. Worthy of special attention is that even cathode sheath thickness in the glow discharge, d_c, is non-constant over the cross-section. This implies that the cathode sheath is not self-contained and independent of the rest of that plasma. Some ions come to the cathode from the plasma and produce secondary electron emission from the cathode surface. Correspondingly, the particle density distributions as well as the ion current in the cathode sheath and on the cathode surface are not transversally uniform as it is assumed in usual 1D models. The absolute value of current streamlines in the cathode sheath, as well as in the plasma, decreases from the center axis of the discharge to the periphery. In turn, this leads to transverse inhomogeneity of the ion current density on the cathode surface. Correspondingly, profile of ionization by fast electrons, originated in the cathode layer, is also non-homogeneous in the transverse direction (see Fig. 6(b)). Figure 6(c) shows profiles of the particle densities (ion, slow, and fast electron) in transverse y direction through points $x = 0.25$, 0.5, and 0.75 cm. The transverse profiles of the ionization function through these points closely resemble those of fast electrons (not shown in the figure).

Thus, the correct condition for the discharge self-maintenance depends not only on the ionization characteristics of the cathode sheath, as assumed in the local models, but also on the parameters of the plasma region.

Analysis performed in Refs. 3 and 5 has shown that the multidimensional geometry leads to the emergence of vortex electric currents in plasmas even in the absence of the magnetic field. These vortex currents reveal themselves, in particular, in violation of the ambipolarity condition, $\Gamma_{i,y} = \Gamma_{e,y}$,

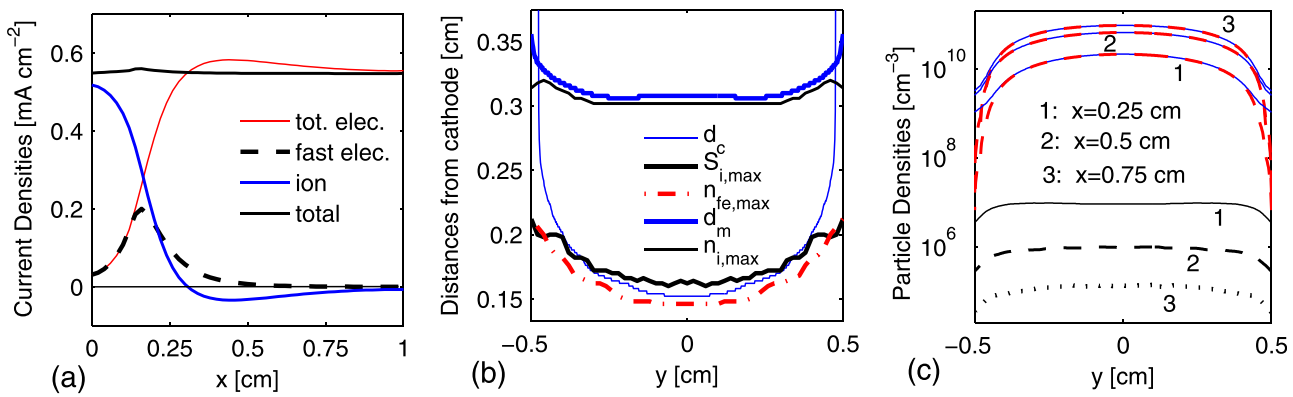

FIG. 6. 2D hybrid model. (a) Profiles of averaged in transversal y direction x components of the total electron, fast electron, ion, and total current densities; (b) cathode sheath thickness d_c, field reversal point d_m, and local maximums of ionization function and ion, slow electron, and fast electron densities as functions of transverse coordinate y; (c) profiles of ion, slow electron, and fast electron densities in transverse y direction through points $x = 0.25$, 0.5, and 0.75 cm.

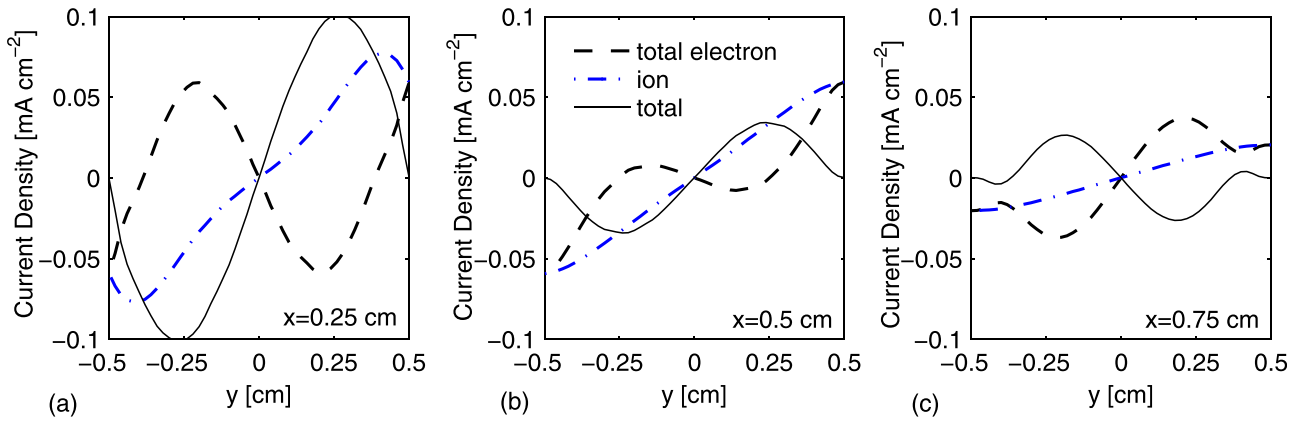

FIG. 7. 2D hybrid model. Profiles of transverse y–components of electron, ion, and total current densities in transverse y direction through points (a) $x = 0.25$, (b) 0.5, and (c) 0.75 cm.

for transverse components of electron and ion fluxes, as can be seen from Fig. 7. This figure contains profiles of transverse y components of the electron, ion, and total current density in the transverse direction through points $x = 0.25$, 0.5, and 0.75 cm. As can be seen, the electron and ion fluxes are not equal to one another, these coincide on the dielectric wall, where the current density vanishes (since it cannot flow through the dielectric).

The current magnitudes and streamlines are presented in Fig. 8. This figure shows the magnitudes and flows of the total electron current density (panel a), the ion current density (panel b), the total current density (panel c), and panel (d) illustrates the vortex current pattern. The vortex current phenomena were predicted theoretically and identified numerically in Ref. 3 in the case of currentless plasma of the ICP discharge. To obtain Fig. 8(d), we used the same approach as in Ref. 5: the mean current density over the cathode surface $\tilde{J}_{x0}$ has been subtracted from the axial component of the current density, $(J_x - \tilde{J}_{x0}, J_y)$, to develop a flow pattern nearly corresponding to a currentless plasma. Condition for emergence of vortex electric currents, which is equivalent to the condition that vectors ∇n and ∇T_e are not parallel, is due to nonuniformity of electron transport coefficients in the dc discharge plasma (see Refs. 3 and 5 for detail). Thus, the vortex formation results from the fundamental nonambipolarity of gas discharge plasmas.

IV. CONCLUSIONS

The two-dimensional (2D) hybrid Monte Carlo–fluid numerical code is developed and applied to study properties of the dc-driven glow discharge. The model is based on separation of electrons into low energetic (slow) and high energetic (fast) groups. The slow electrons and ions are described by the fluid model. Fast electrons, simulated by the particle method, are responsible for ionization processes in the

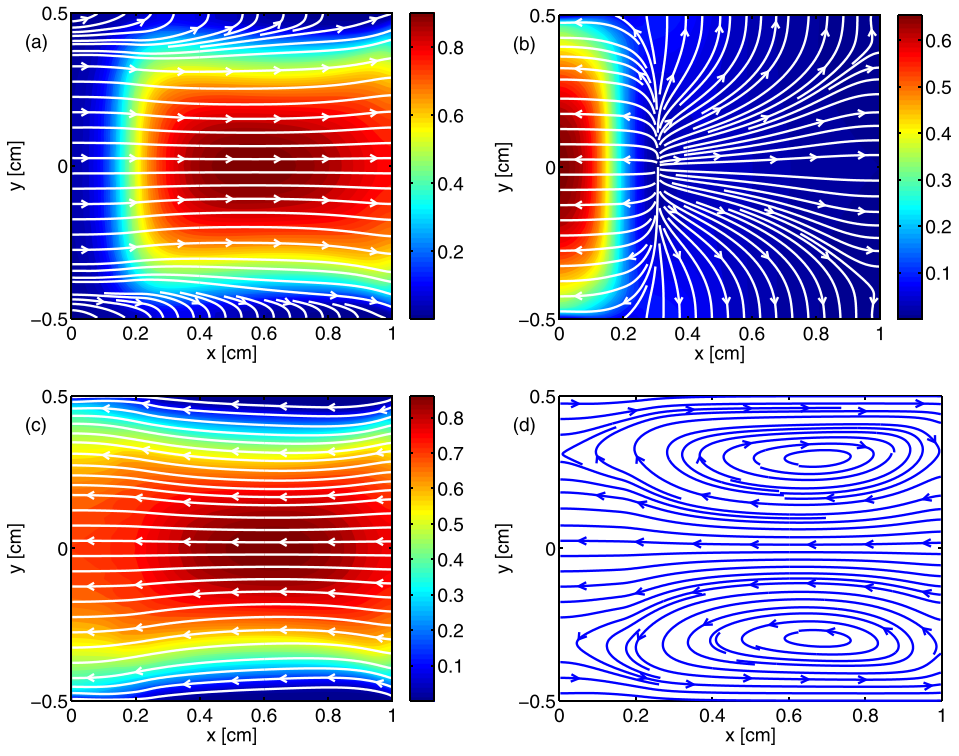

FIG. 8. 2D hybrid model. (a) Total electron current density (colored) and current flow (streamlines), (b) ion current density (colored) and current flow (streamlines), (c) total electric current density (colored) and current flow (streamlines), (d) vortex current flow. $p = 1$ Torr, $T_e = 1$ eV, $\gamma = 0.06$, $L_x = 1$ cm, $L_y = 1$ cm, $V_a = 250$ V.

discharge, which are taken into account by the Monte Carlo collision method. Electrostatic field is obtained from the solution of the Poisson equation.

For a validation of the numerical code, we first performed calculations under conditions studied in Ref. 9 within 1D model. The results were found to be in perfect agreement with those from Ref. 9.

Basic properties of the glow discharge sustained in argon gas (such as spatial profiles of charged particle densities, electric field, and ionization source function) were studied. Current-voltage characteristics (CVC) were obtained from 1D and 2D hybrid models and compared with computed CVC from 1D study Ref. 7 and measured CVC's from Refs. 31 and 32. Electric field reversal phenomena and vortex current formation were investigated. Computed results from the simple fluid and extended fluid models were also considered and discussed.

Two methods are shown to be workable to model glow discharges: extended fluid model and hybrid model. Contrary to reports in the literature (see, e.g., Ref. 9), the analysis does not reveal significant advantages of the hybrid method (which is non self-consistent as long as the electron energy balance equation is not included into the system) over the extended fluid model.

In connection with the above discussion, the idea which suggests itself is a combination of the hybrid and the extended fluid model into one model, which will incorporates the advantages of these models and eliminate their shortcomings. Within such a model, the non-local ionization will be derived from the Monte Carlo simulation of fast electron kinetics, while the slow electron transport parameters will be obtained as functions of the temperature, determined from the energy balance of slow electrons.

ACKNOWLEDGMENTS

The work was supported by research Grant Nos. 210T072 and 212T164 from the Scientific and Technical Research Council of Turkey (TUBITAK). A.A.K. thanks RFBR (Grant No. 13-02-91375 CTa) and SPSU (Grant No. 11.38.658.2013) for the support.

[1]Y. P. Raizer, *Gas Discharge Physics* (Springer-Verlag, Berlin, 1991).
[2]V. I. Kolobov and L. D. Tsendin, Phys. Rev. A **46**, 7837 (1992).
[3]E. A. Bogdanov, A. S. Chirtsov, and A. A. Kudryavtsev, PRL **106**, 195001 (2011).
[4]Z. Donko, Plasma Sources Sci. **20**, 024001 (2011).
[5]I. R. Rafatov, E. A. Bogdanov, and A. A. Kudryavtsev, Phys. Plasmas **19**, 033502 (2012).
[6]J. P. Vorbencoeur, Plasma Phys. Controlled Fusion **47**, 231 (2005).
[7]Z. Donko, P. Hartmann, and K. Kutasi, Plasma Sources Sci. Technol. **15**, 178 (2006).
[8]G. J. M. Hagelaar and L. C. Pitchford, Plasma Sources Sci. Technol. **14**, 722 (2005).
[9]A. Derzsi, A. Hartmann, I. Korolov, J. Karacsony, G. Bano, and Z. Donko, J. Phys. D: Appl. Phys. **42**, 225204 (2009).
[10]I. Rafatov, E. A. Bogdanov, and A. A. Kudryavtsev, Phys. Plasmas **19**, 093503 (2012).
[11]J. P. Boeuf and L. C. Pitchford, Phys. Rev. E **51**, 1376 (1995).
[12]R. R. Arslanbekov and A. A. Kudryavtsev, Phys. Rev. E **58**, 6539 (1998).
[13]R. R. Arslanbekov and A. A. Kudryavtsev, in *Electron Kinetics and Applications of Glow Discharges*, NATO ASI Series B: Physics Vol. 367, edited by U. Kortshagen and L. D. Tsendin (Plenum Press, New York, 1998), pp. 161–178.
[14]R. R. Arslanbekov, A. A. Kudryavtsev, and R. C. Tobin, J. Appl. Phys. **81**, 554 (1997).
[15]R. R. Arslanbekov, A. A. Kudryavtsev, and R. C. Tobin, Plasma Sources Sci. Technol. **7**, 310 (1998).
[16]R. R. Arslanbekov and A. A Kudryavtsev, Phys. Plasmas **6**, 1003 (1999).
[17]A. A. Kudryavtsev, A. V. Morin, and L. D. Tsendin, Tech. Phys. **53**, 1029 (2008).
[18]R. Arslanbekov and V. Kolobov, J. Phys. D: Appl. Phys. **36**, 2986 (2003).
[19]C. K. Birdsall, IEEE Trans. Plasma Sci. **19**, 65 (1991).
[20]A. Fiala, L. C. Pitchford, and J. P. Boeuf, Phys. Rev. E **49**, 5607 (1994).
[21]M. Surendra, D. B. Graves, and G. M. Jellum, Phys. Rev. A **41**, 1112 (1990).
[22]A. Bogaerts and R. Gijbels, Phys. Rev. A **52**, 3743 (1995).
[23]J. P. Boeuf and L. C. Pitchford, IEEE Trans. Plasma Sci. **19**, 286 (1991).
[24]See http://www.lxcat.laplace.univ-tlse.fr for "PHELPS database" (retrieved August 27, 2013).
[25]S. V. Patankar, *Numerical Heat Transfer and Fluid Flow* (McGraw-Hill, New York, 1980).
[26]S. Jardin, *Computational Methods in Plasma Physics* (Taylor & Francis, London and New York, 2010).
[27]E. W. McDaniel, *Collision Phenomena in Ionized Gases* (Wiley, New York, 1964).
[28]L. S. Frost, Phys. Rev. **105**, 354 (1957).
[29]E. A. Bogdanov, S. F. Adams, V. I. Demidov, A. A. Kudryavtsev, and J. M. Williamson, Phys. Plasmas **17**, 103502 (2010).
[30]Z. Donko, Phys. Rev. E **64**, 026401 (2001).
[31]K. Rozsa, A. Gallagher, and Z. Donko, Phys. Rev. E **52**, 913 (1995).
[32]I. Stefanovic and Z. Lj. Petrovic, Jpn. J. Appl. Phys., Part 1 **36**, 4728 (1997).